 CMES, vol.3, no.4, pp.483-495, 2002

Steady-State Temperature Rise in Coated Halfspaces and Halfplanes

Michael J. Rodgers[1], Leon M. Keer, and Herbert S. Cheng

Abstract: The steady-state temperature rise due to frictional heating on the surface of coated halfspaces and halfplanes is described by closed form expressions in the Fourier transformed frequency domain. These frequency response functions (FRFs) include the effects of the coating and the speed of the moving heat source and apply for all Peclet number regimes. Analytical inversion of these expressions for several special cases shows the Green's functions as infinite series of images, which may be costly and slowly convergent. Also, the influence coefficients integrated from these Green's functions are not available in closed form. Applying fast Fourier transform (FFT) methods to invert the frequency domain expressions does not rely on the infinite summations, and the influence coefficients can be computed quickly and accurately. The accuracy for several FFT methods are analyzed in comparison with available homogeneous cases (halfspace: low Peclet and high Peclet number approximations; halfplane: all Peclet numbers, as well as low and high Peclet number approximations). Finally, a brief parameter study about the effect of the coating is performed, using the discrete convolution fast Fourier transform (DC-FFT) algorithm for accurate and efficient calculations of the temperature rise from the frequency response functions.

1 Introduction

Frictional heating can lead to hot spots that cause decreased performance and failure in machine parts. This important field has been studied for many decades, beginning with the pioneering work of Blok (1937, 1963), Jaeger (1942) and Archard (1958). The classic *Conduction of Heat in Solids* (Carslaw and Jaeger, 1959) forms the basis of practically every study in this field, including this work. Here, frictional heating is studied on a tribological scale relevant to tribological elements with thin protective coatings because developments in coating technology hold much promise for increased tribological performance.

Many models of tribological coatings and frictional heating have used finite element analysis [e.g. Kennedy, Colin, Floquet and Glovsky (1984); Liu and Wang (1999)]. These studies are proving to be useful in virtual tribology, especially if they can be used as a preprocessing step and if the fast Fourier transform (FFT) can be used in the main analysis [(Liu, Wang and Liu (2001)]. Other studies include the boundary element method (BEM) study by Vick, Golan and Furey (1994), which shows that the BEM also holds promise as an appropriate method for contact analysis.

Ling (1973) used Fourier analysis for temperature rise and thermoelasticity. The work of Ju and Farris (1997) showed that FFT could be applied to problems with moving heat sources. This study follows those works and the work of Tian and Kennedy (1993, 1994), which developed approximate formulas, over the whole range of Peclet number, for temperature rise in moving bodies – formulas that proved to be good when tested against finite element simulations. The formulas of Tian and Kennedy (1993) were also used in a flash temperature analysis of journal bearings [Wang and Cheng (1995)]. Other important papers that use FFT in regard to tribological coatings include Floquet (1985) and Leroy, Floquet and Villechaise (1989, 1990).

The notion of flash temperature refers to the hot spots of two bodies in contact, and therefore, heat partitioning between the two bodies is the essential consideration. Recent studies of heat partitioning and flash temperature include Bos and Moes (1995), Qui and Cheng (1998) and Gao, Lee, Ai and Nixon (2000). The latter paper uses FFT techniques to study transient heat conduction and to calculate the temperature fields and the heat partition function for rough surfaces in contact. The FFT, then, has been shown to be quite useful in studying both rough

[1] Center for Surface Engineering and Tribology
Northwestern University
Evanston, IL 60208, USA
847-491-9902; 847-491-4011(fax); m-rodgers@northwestern.edu

contact and coated contact. Here, this usefulness is expanded by demonstrating the potential for fast heat partition solvers to study coated bodies in rough contact and by using the discrete-convolution fast Fourier transform (DC-FFT) method, first introduced for contact solvers by Liu, Wang and Liu (2000).

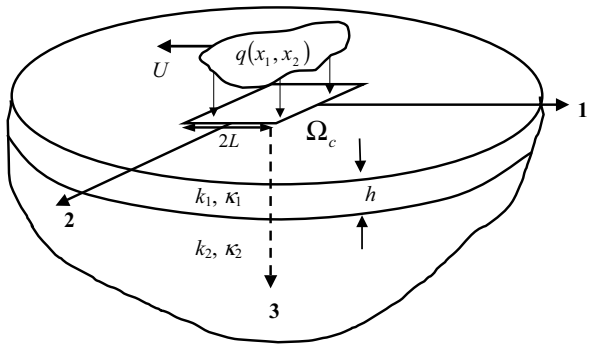

Figure 1 : Model and Geometery. The surface heat source $q(x_1,x_2)$ acts in the contact region Ω_c of length $2L$, which is fixed to a coordinate system moving at speed U in the negative x_1 direction. The coating, of thickness h, and substrate have conductivities k_1, k_2 and diffusivities κ_1, κ_2 respectively.

2 Analysis

As shown in Fig. 1, the coordinate system is fixed to the center of the moving heat source. The nondimensionalized differential equations

$$\nabla^2 T_j = 2P_j \partial_1 T_j, \qquad j=1,2, \qquad \text{no summation,} \quad (1)$$

where $\nabla^2 = \partial_1^2+\partial_2^2+\partial_3^2$, $\partial_k = \partial/\partial x_k$ $(k=1,2,3)$, and P_j is the Peclet number, govern the nondimensional steady-state temperature changes $T_j(x_1,x_2,x_3)$ in the coating $(j=1,\ 0<x_3<h)$ and substrate $(j=2,\ h<x_3)$ respectively, where h is the coating thickness. The nondimensional heat source $q(x_1,x_2)$ is generated in the contact region Ω_C and is assumed to vanish outside of this region:

$$-\partial_3 T_1|_{x_3=0} = \begin{cases} q(x_1,x_2), & (x_1,x_2)\in\Omega_C \\ 0, & (x_1,x_2)\notin\Omega_C \end{cases} \quad (2)$$

The coating is perfectly bonded to the substrate so that both the heat flux and the temperature are continuous at $x_3=h$. Nondimensionalization in Eqs. (1) and (2) was achieved by

$$T_j = \frac{\overline{T}_j k_j}{Lq_0}, \quad j=1,2, \text{no summation,} \quad (3a)$$

$$x_m = \frac{\overline{x}_m}{L}, \quad m=1,2,3, \quad (3b)$$

$$h = \overline{h}/L, \quad q = \overline{q}/q_0, \quad (3c)$$

$$P_j = \frac{UL}{2\kappa_j}, \quad j=1,2, \quad (3d)$$

where q_0 is the maximum heat flux, L is a half-length of the heat source, U is the speed, κ_j is the diffusivity and k_j is the conductivity, all assumed constant.

Equations (1) – (2) are solved by Fourier transform techniques, and the transformed nondimensional temperature changes $\tilde{\tilde{T}}_j(\omega_1,\omega_2,x_3)$ are found to be

$$\tilde{\tilde{T}}_j(\omega_1,\omega_2,x_3) = \tilde{\tilde{g}}_j(\omega_1,\omega_2,x_3)\ \tilde{\tilde{q}}(\omega_1,\omega_2), \quad j=1,2, \quad (4)$$

where the frequency response functions (FRF) are

$$\tilde{\tilde{g}}_1 = \frac{1}{\eta_1}\left[\exp(-\eta_1 x_3) + \frac{(k_1\eta_1-k_2\eta_2)\exp(-\eta_1 h)}{k_1\eta_1\sinh(\eta_1 h)+k_2\eta_2\cosh(\eta_1 h)}\cosh(\eta_1 x_3)\right], \quad (5a)$$

$$\tilde{\tilde{g}}_2 = \frac{k_2\exp[-\eta_2(x_3-h)]}{k_1\eta_1\sinh(\eta_1 h)+k_2\eta_2\cosh(\eta_1 h)}, \quad (5b)$$

where $\eta_j = \sqrt{\omega_1^2+\omega_2^2-2\mathrm{i}P_j\omega_1}$, $j=1,2$. In Eqs. (4) – (5), each $\tilde{}$ implies a Fourier transform and ω_1, ω_2 are the angular frequencies corresponding to the nondimensional x_1, x_2 (See Appendix). Similar expressions to Eq. (5) have been derived in the literature [c.f. Ju and Liu (1988); Leroy, Floquet and Villechaise (1989, 1990)].

Equation (5a) shows that the FRF for the coating contains the sum of the halfspace FRF and a correction FRF: $\tilde{\tilde{g}}_1 = \tilde{\tilde{g}}_1^{HS} + \tilde{\tilde{g}}_1^{C}$. The correction FRF vanishes when the solid is homogeneous, i.e. when both $k_1=k_2$ and $\kappa_1=\kappa_2$ or when $h\to\infty$. The Green's functions g and the influence coefficient G for several cases for the homogeneous body are presented next, because these will be used to describe the accuracy of the FFT based methods and because the effect of the coating is considered as a correction effect from the halfspace solutions.

2.1 Homogeneous Case

For point contact, the halfspace FRF and Green's function are

$$\tilde{g}_1^{HS}=\frac{\exp(-\eta_1 x_3)}{\eta_1},\quad g_1^{HS}(x_1,x_2,x_3)=\frac{\exp[-P_1(\rho-x_1)]}{2\pi\rho}, \tag{6}$$

where $\rho^2=x_1^2+x_2^2+x_3^2$ [Carslaw and Jaeger (1959); Ling (1973)]. Analytical expressions for the influence coefficients have not been found analytically in the literature for arbitrary Peclet numbers. For low Peclet numbers ($P_1\sim 0$), the influence coefficients G are

$$G^{HS}(x_1,x_2,0)=f(x^+,y^+)+f(x^-,y^-)-f(x^+,y^-)-f(x^-,y^+) \tag{7a}$$

$$f(x_1,x_2)=x_1\ln(x_2+r)+x_2\ln(x_1+r) \tag{7b}$$

$$x^+=x_1+\Delta_1/2,\quad x^-=x_1-\Delta_1/2,$$
$$y^+=x_2+\Delta_2/2,\quad y^-=x_2-\Delta_2/2, \tag{7c}$$

where $r^2=x_1^2+x_2^2$ and where Δ_1, Δ_2 define the nodal spacing in the x_1, x_2 directions [Johnson (1985)]. For high Peclet numbers($P_1\gg 1$), the heat source moves faster than the heat is conducted, so that $\eta_1=\sqrt{\omega_2^2-2iP_1\omega_1}$. Equations (6) – (7) apply, but with

$$g_1^{HS}(x_1,x_2,x_3)=\frac{H(x_1)}{2\pi x_1}\exp\left[-\frac{P_1\left(x_2^2+x_3^2\right)}{2x_1}\right], \tag{8a}$$

$$f(x_1,x_2)=H(x_1)\left[\sqrt{\frac{x_1}{2\pi P_1}}\mathrm{erf}\left(x_2\sqrt{\frac{P_1}{2x_1}}\right)-\frac{x_2}{2\pi}Ei\left(-\frac{x_2^2P_1}{2x_1}\right)\right], \tag{8b}$$

where $H(u)$ is the Heaviside unit step function, erf(u) is the error function and Ei(-u) is the exponential integral function [Tichy (1991)].

For line contact, $\omega_2=0$, $\eta_1=\sqrt{\omega_1^2-2iP_1\omega_1}$, and the Green's function g and the influence coefficient G for the halfplane are

$$g_1^{HP}(x_1,x_3)=\int_{-\infty}^{+\infty}g_1^{HS}(x_1-\xi_1,0-\xi_2,x_3)\,d\xi_2$$
$$=\frac{1}{\pi}\exp(P_1x_1)\,K_0(P_1d), \tag{9a}$$

$$G^{HP}(x_1,0)=\frac{1}{\pi P_1}\left[f^-(-P_1x^-)H(-x^-)-f^-(-P_1x^+)H(-x^+)+f^+(P_1x^+)H\left(x^+\right)-f^+(P_1x^-)H\left(x^-\right)\right] \tag{9b}$$

$$f^{\pm}(u)=\int_0^u\exp(\pm u)\,K_0(u)\,du$$
$$=u\exp(\pm u)\left[K_0(u)\pm K_1(u)\right]\mp 1, \tag{9c}$$

where $d^2=x_1^2+x_3^2$, $K_n(u)$ is the modified Bessel function of the second kind of order n, and x^+,x^- are given by Eq. (7c) [Carslaw and Jaeger (1959)]. Also, separate expressions for the low and high Peclet number regimes are found in the literature. For low Peclet numbers ($P_1\sim 0$), a bulk logarithmic infinity in Eq. (9) [c.f. Carslaw and Jaeger (1959), Ling (1973)] can be ignored by the consideration of an appropriate reference point [c.f. Johnson (1985)]. Then, the Green's function g and the influence coefficient G are

$$g_1^{HP}(x_1,x_3)=-\frac{1}{\pi}\ln d, \tag{10a}$$

$$G^{HP}(x_1,0)=f\left(x^+\right)-f\left(x^-\right), \tag{10b}$$

$$f(x_1)=\frac{1}{\pi}x_1\left(\ln|x_1|-1\right), \tag{10c}$$

where x^+,x^- are given by Eq. (7c). For high Peclet numbers($P_1\gg 1$), the heat source moves faster than the heat is conducted, so that $\eta_1=\sqrt{-2iP_1\omega_1}$. The Green's function g for this case is [Tichy (1991)]:

$$g_1^{HP}(x_1,x_3)=\frac{1}{\sqrt{2\pi P_1x_1}}\exp\left(-\frac{x_3^2P_1}{2x_1}\right),\quad x_1>0 \tag{11}$$

The influence coefficient G for this half-plane case is

$$G^{HP}(x_1,x_3)=f\left(x^+,x_3\right)-f\left(x^-,x_3\right), \tag{12a}$$

$$f(x_1,x_3) = H(x_1)\left[x_3 \operatorname{erf}\left(x_3\sqrt{\frac{P_1}{2x_1}}\right) + \sqrt{\frac{2x_1}{\pi P_1}}\exp\left(-\frac{x_3^2 P_1}{2x_1}\right)\right], \tag{12b}$$

where x^+, x^- are given by Eq. (7c). For the surface $x_3 = 0$, Eq. (12) was found by Tichy (1991).

2.2 Coated Case

For analytical inversion of the coating's correction FRF and the substrate's FRF from Eq. (5), the series expansion technique gives

$$\tilde{\tilde{g}}_1^C = \frac{2S}{\eta_1}\cosh(\eta_1 x_3) \tag{13a}$$

$$\tilde{\tilde{g}}_2 = \frac{2k_2}{k_1\eta_1 + k_2\eta_2}(1+S)\exp[-\eta_2 x_3 - h(\eta_1 - \eta_2)] \tag{13b}$$

$$S = \sum_{m=1}^{\infty} R^m \exp(-2\eta_1 hm), \tag{13c}$$

$$R = \frac{k_1\eta_1 - k_2\eta_2}{k_1\eta_1 + k_2\eta_2} \tag{13d}$$

The terms S and R are defined as the correction sum and the parameter ratio, respectively. Clearly, the parameter ratio ranges between $-1 < R \leq 1$, and for a homogeneous body $R = S = 0$. Similar expressions to Eq. (13), which represents a series of images in the frequency domain, have been derived in the literature [Ling (1973); Tian (1992); Tian and Kennedy (1993)].

When the parameter ratio is independent of the frequencies (ω_1, ω_2), it may be possible to invert Eq. (13) analytically through term by term integration [e.g. Carrier and Pearson (1988)]. For example, the matching diffusivity case has $\kappa_1 = \kappa_2$ and $R = \dfrac{k_1 - k_2}{k_1 + k_2}$. The Green's functions for point and line contact can be found term by term using Eqs. (A4) – (A5). Another example is the heated slab case, which has $k_2 = 0$ and $R = 1$. While the Green's functions g_2 are meaningless when $k_2 = 0$, the Green's functions g_1 for the coating (slab) can be found by the same process as those for the matching diffusivity case. Since influence coefficients are not available for the general halfspace (or halfplane) case when $x_3 \neq 0$, influence coefficients cannot be found for either of these two (matching diffusivity and heated slab) examples. A third example, though, does have closed form influence coefficients. For the fast-moving line contact case $(P_1, P_2 >> 1)$, the parameter ratio R is given by $R = \dfrac{k_1/\sqrt{\kappa_1} - k_2/\sqrt{\kappa_2}}{k_1/\sqrt{\kappa_1} + k_2/\sqrt{\kappa_2}}$. The coating's correction Green's function is given by

$$g_1^C(x_1,x_3) = g_1^{HP}(x_1,x_3)\sum_{m=1}^{\infty} R^m\left[\exp\left(\frac{-P_1 z_m^+}{2x_1}\right) + \exp\left(\frac{-P_1 z_m^-}{2x_1}\right)\right] \tag{14}$$

where $z_m^{\pm} = 4hm(hm \pm x_3)$ and $g_1^{HP}(x_1,x_3)$ is given by Eq. (11). The substrate's Green's function is given by

$$g_2(x_1,x_3) = \frac{2k_2/\sqrt{\kappa_2}}{k_1/\sqrt{\kappa_1} + k_2/\sqrt{\kappa_2}} \cdot g_2^{HP}(x_1,x_3)\left[\exp\left(\frac{-z_0}{2x_1}\right) + \sum_{m=1}^{\infty} R^m \exp\left(\frac{-z_m}{2x_1}\right)\right] \tag{15}$$

where $z_m = hP'_m\left(hP'_m + 2x_3\sqrt{P_2}\right)$, $P'_m = (1+2m)\sqrt{P_1} - \sqrt{P_2}$, and $g_2^{HP}(x_1,x_3)$ is given by Eq. (11), with the substitution of P_2 for P_1. Equation (14) reduces to the result by Ling (1973) for the surface $(x_3 = 0)$ temperature rise. Influence coefficients can be found in closed form through term by term integration of the form given by Eq. (12). The expressions are lengthy and are not reported here.

In summary, the frequency response functions (FRFs) are known for all cases of Peclet number for both the coated halfspace and the coated halfplane. Influence coefficients are known for many, but not all cases. For the cases with known influence coefficients, calculations using the FRFs in FFT based methods are compared to calculations with these influence coefficients. Methods that use these expressions and FFT to perform these calculations are described in the next section.

3 FFT Method

For an arbitrary applied heat flux, solution of Eq. (4) can be calculated quickly by using the FFT and by assuming

that the heat flux is constant over elements that subdivide the contact region. These elements must be in a rectangular grid, with a power of 2 number of elements in each direction. Refinement of the grid can occur only by increasing the number of grids to a higher power of 2 in each direction, and thus, the grid must be refined in entirety, and not in specific locations of interest. Despite these restrictions, FFT methods hold much promise for tribological contact problems because of the small number of required operations, as compared with direct multiplication methods. Also, enhanced FFT methods that calculate transforms from real data by exploiting complex conjugate symmetries are readily available [Press, Teukolsky, Vetterling and Flannery (1992)]. However, the FFT, which is a clever algorithm for exactly calculating the discrete Fourier transform [Stein (1997)], involves periodicity concerns which must be addressed. In this light, three FFT-based approaches used here are discussed next.

Since the frequency response functions (FRFs) are available, they can be used directly in an FFT-based approach to obtain the temperature rise, by transforming the applied heat flux into the frequency domain, multiplying with the FRF point by point, and inverting the result into the spatial (target) domain. If the analytical transform of the applied heat flux is available, it can be used in Eq. (4); otherwise the heat flux can be transformed by FFT into the frequency domain first. Note that the infinite term in the frequency response functions $[\tilde{g}(\omega_1 = \omega_2 = 0) \to \infty]$ must be discarded, and that this causes the loss of bulk information [Liu, Wang and Liu (2000)]. Numerical or analytical integration around this singular point may be used to retrieve this lost information, but researchers can often consider a reference point and/or a physical argument to set the bulk.

The above inverse FFT (IFFT) method, which uses the continuous convolution theorem, should be applied directly to Eq. (4) with a frequency refinement factor M of at least 8 to diminish the aliasing (periodicity) error [Polonsky and Keer (2000); Liu, Wang and Liu (2000)]. This refinement factor gives the frequency step size to be $\Delta\omega_1 = 2\pi/NM\Delta_1$, where N is the number of elements in the target domain (both N and M must be powers of 2). For example, consider the homogeneous line contact case, with a length patch of constant heat flux $q = 1$ over $-1 \le x_1 \le 1$, and where $P_1 = 1$ and $N = 128$. This heat flux has an analytical Fourier transform $\tilde{q} = 2\sin(\omega_1)/\omega_1$. In Fig. 2, the surface $x_3 = 0$ temperature rise results for this example show that the periodicity effects are significantly diminished as the frequency refinement factor $M \ge 8$. The dashed curves show the IFFT result with M as indicated, while the solid curve shows the analytical solution of Eqs. (9b) – (9c), with $x^+ = x_1 + 1, \quad x^- = x_1 - 1$. Note that the bulk is set for each IFFT curve by setting the IFFT equal to the analytical at the reference point $x_1 = -3$. The case with $M = 1$ shows complete periodicity, as the curve can be seen to leave the frame at $x_1 = 3$ and to return in step at $x_1 = -3$. The cases with $M \ge 8$ show improved accuracy that diminishes slightly towards the right of the frame.

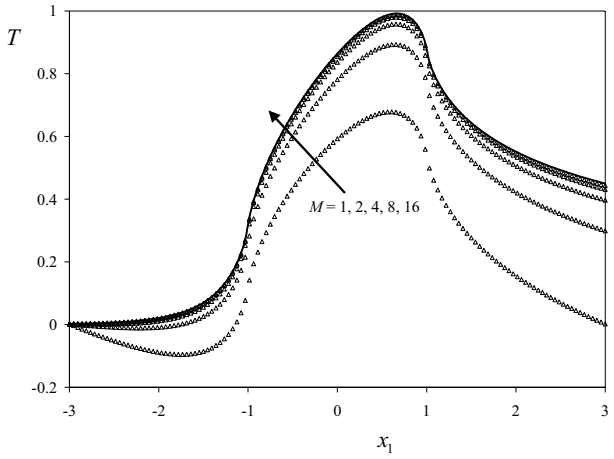

Figure 2 : Periodicity correction by frequency refinement. The triangles show the IFFT results for the line source case with $P = 1$, plotted for different values of M, the frequency domain refinement factor. The analytical solution is the solid line.

The frequency refinement corresponds to expansion in the spatial domain, and, clearly, this frequency refinement is not necessary in periodic problems [Polonsky and Keer (2000); Liu, Wang and Liu (2000); Colin and Lubrecht (2001)]. In a nonperiodic contact problem, the contact solver algorithm [e.g. Polonsky and Keer (1999)] and the heat partition algorithm [e.g. Bos and Moes (1995)] have many iteration steps, and the refined frequency (or expanded spatial) domain required to reduce the aliasing error in the IFFT method would slow down the computation speed dramatically and unnecessarily. At each iteration step, the discrete convolution theorem should be used with the influence coefficients G, because the computational domain required to completely avoid

aliasing error is only twice as large as the target domain [Press, Teukolsky, Vetterling and Flannery (1992); Liu, Wang and Liu (2000)]. To use the discrete convolution FFT algorithm, special attention must be placed both on the wrap-around order for the influence coefficients and on the zero padding for the applied heat flux. Wrap-around order refers to the standard FFT process of placing all the negative values of the array after the positive values; zero padding refers to the standard FFT process of zeroing all nodes outside the target domain [Press, Teukolsky, Vetterling and Flannery (1992)].

The influence coefficients are needed for the discrete convolution at every iteration step, and therefore, they should be found in a preprocessing algorithm, either by inverse FFT from the frequency response functions (FRF method) or by integration of the Green's function over constant patches of applied heat flux (IC method). If the influence coefficients are available in closed form, then the closed form expressions should be used. Closed form expressions for several cases were presented in the previous sections. The FRF method for determining the influence coefficients for the line contact problem is described next.

Numerical influence coefficients are found in the FRF method by inverting the line contact frequency response functions, which are given by Eq. (5), with $\omega_2 = 0$. The patch has length equal to the node spacing Δ_1, and it is centered at the origin. Thus, the transform domain influence coefficient is

$$\tilde{G}(\omega_1) = \tilde{g}\sin(\omega_1\Delta_1/2)\,/\,(\omega_1/2) \tag{16}$$

The three FFT-based methods can be summarized as follows. The IFFT method, which utilizes the continuous convolution theorem, applies for periodic problems, with no expanded domain, and for nonperiodic problems, with an expanded domain (or frequency refinement) by at least 8 times. The FRF method and the IC method utilize the discrete convolution theorem and, therefore, rely on the influence coefficients, which are found by IFFT in the FRF method or by analytical (or other numerical) means in the IC method. Using the FFT with the discrete convolution theorem produces no additional periodicity error. In this light, the three methods are applied to specific problems in the next section.

4 Results

In this section, the results from the FFT methods are presented and discussed. For the halfspace cases, the surface of the halfspace is discretized into a grid, with 128 nodes in each direction that are spaced from $-3 \le x_1 \le 3$, $-3 \le x_2 \le 3$, giving $\Delta_1 = \Delta_2 = 0.046875$. For the FRF method, the frequency refinement factor M is chosen to be 8, in each direction, while for the IFFT method $M = 16$. The IFFT method requires more refinement because the FRF method has heat input over only one element. The halfplane cases use the same values, but the discretization is in the x_1 direction only.

Note that the discretization alone produces errors because even simple heat sources will not be perfectly described by square patches of constant heat flux. The different FFT methods were applied to simple cases for the heat flux, for both the point contact and line contact cases, and the results are presented next.

4.1 Homogeneous Case: Circular Patch

The FFT methods are applied to the halfspace case Eq. (6) to find the surface $x_3 = 0$ temperature rise due to a constant heat input over a circular patch of nondimensional radius a. To set the bulk temperature rise, which is lost in the FFT methods, an analytical result presented next. For observation points (r,θ) inside a circular patch of radius a, the integration becomes

$$T_1^{HS}(x_1,x_2,0) = \int_{-\pi}^{+\pi}\int_0^{s'} \exp\left[-P_1 s\,(1+\cos\psi)\right] ds\,d\psi \tag{17}$$

where

$$s = \sqrt{(x_1-\xi_1)^2+(x_2-\xi_2)^2},$$
$$\xi_1 - x_1 = s\cos\psi, \quad \xi_2 - x_2 = s\sin\psi \tag{18a}$$

$$s' = -r\cos(\psi-\theta) + \sqrt{a^2 - r^2\sin^2(\psi-\theta)} \tag{18b}$$

$$r = \sqrt{x_1^2+x_2^2}, \quad x_1 = r\cos\theta, \quad x_2 = r\sin\theta \tag{18c}$$

This polar coordinate transformation is used in Johnson (1985) for pressure on a halfspace. Here, the integration is not axisymmetric because of the motion of the heat source in the x_1 direction. For observation at the center

$(r=0)$ of the circular patch, analytical integration gives [Abramowitz and Stegun (1972)]:

$$T_1^{HS}(0,0) = 2\pi a \exp(-P_1 a)\left[I_0(P_1 a) + I_1(P_1 a)\right] \qquad (19)$$

where $I_n(u)$ is the modified Bessel function of the first kind of order n. Typical values for Eq. (19), for $a=1$, are $T_1^{HS}=1$, 0.9524, 0.6737, 0.3475 and 0.2491, for $P_1=0$, 0.1, 1, 5 and 10, respectively. For all other observation points (inside or outside the circular patch) closed form expressions are not available.

The IFFT and FRF methods are used for the general case of arbitrary Peclet number. For the IFFT method, note that the heat flux has an analytical transform for this case, found by direct integration, using a polar coordinate system that takes advantage of the relation between Fourier transforms and Hankel transforms [Sneddon (1951)], giving

$$\tilde{\tilde{q}}(\omega_1,\omega_2) = 2\pi \int_0^a J_0(rw)\, r\, dr = \frac{2\pi a}{w} J_1(aw) \qquad (20)$$

where $w^2 = \omega_1^2 + \omega_2^2$ and $J_n(u)$ is the Bessel function of the first kind of order n. Also, the methods are compared to an IC method, which uses numerical and analytical integration applied to the following form of Eq. (17), which isolates the singular point:

$$G_1^{HS}(x_1,x_2,0) = \iint \frac{\exp\{-P_1[(s-(x_1-\xi_1))]\}-1}{s} d\xi_1\, d\xi_2 + \iint \frac{1}{s} d\xi_1\, d\xi_2 \qquad (21)$$

The second integral on the right hand side is analytically integrated by Eq. (7), and the first integral will have reasonable accuracy by Simpson's method [Rodgers, 2001]. The area of integration of Eq. (21) is the rectangular patch of Eq. (7), and so the result is used in the discrete convolution theorem algorithm (IC method). Finally, all three FFT methods are compared to the analytical results, which apply for $P_1=0$:

$$T_1^{HS}(x_1,x_2,0) = \frac{2a}{\pi}\mathbf{E}\left(\frac{r}{a}\right), \quad r \le a \qquad (22a)$$

$$T_1^{HS}(x_1,x_2,0) = \frac{2r}{\pi}\left[\mathbf{E}\left(\frac{a}{r}\right) - \left(1-\frac{a^2}{r^2}\right)\mathbf{K}\left(\frac{a}{r}\right)\right], \quad r > a \qquad (22b)$$

where $\mathbf{K}(u)$ and $\mathbf{E}(u)$ are the complete elliptic integral of the first and second kind [Johnson (1985)].

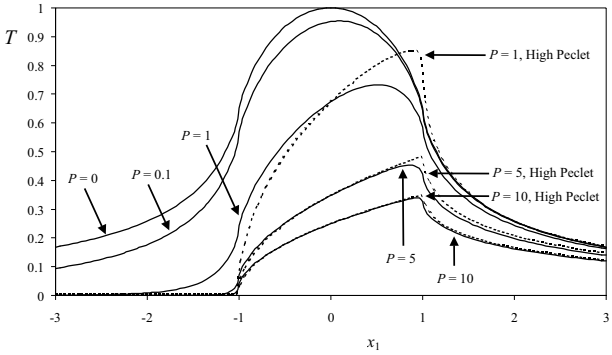

Figure 3 : Homogeneous Pint Contact: Circle Source. The surface temperature rise is plotted vs. x_1 for various Peclet numbers. The solid lines are the FRF method results, while the dashed lines are the IC method results for high Peclet number.

In Fig. 3, several values of $P=P_1$ are used to show the FFT results for the surface $x_3=0$ temperature rise $T=T_1$ vs. x_1, with $x_2=0$. Since the IFFT, FRF and IC results are nearly identical (indistinguishable on a graph like Fig. 3) for each case of Peclet number, only the results from the FRF method are shown for the arbitrary Peclet number case. The high Peclet number solution of Eq. (8), which is used in the discrete convolution theorem algorithm (IC method), is shown in Fig. 3 to be appropriate for $P>5$ or $P \ge 10$. Since the bulk information is lost, all curves (both those from the FRF method and those from the IC method) are set relative to the analytical result from Eq. (19), i.e. relative to the reference point at the origin.

The average absolute errors between pairs of results are given as follows: For $P=0$, this error between the IC method (using Eq. (21), which is completely analytical – Eq. (7) – for $P_1=0$) and the analytical solution of Eq. (22) is 6.9 (10^{-4}). This error is the discretization error of approximating a circle by a rectangular grid. Also, for $P=0$, this error between the FRF method and the analytical solution of Eq. (22) is approximately 7.4 (10^{-4}).

Thus the error of the FRF method is only slightly more than the discretization error, for $P = 0$. For all other values of P, this error between the FRF method and the IC method is less than 1.7 (10^{-4}), and this error between the FRF method and the IFFT method is less than 7.5 (10^{-4}). In conclusion, the error of the FRF method is comparable to that of the IC method, and both methods require the same computational cost, provided that the influence coefficients are calculated in preprocessing.

4.2 Homogeneous Case: Length Patch

The IFFT and FRF methods are applied to the halfplane case to find the surface $x_3 = 0$ temperature rise due to a constant heat input over a length L = 1. For the IFFT method, note that the analytical transform of the heat flux is $\tilde{q}(\omega_1) = 2\sin(\omega_1)/\omega_1$.

Ju and Farris (1997) used IFFT for this problem, with an expanded computational domain of 409.6L (here, 6ML = 96L), a total number of elements of 8192 (here, NM = 2048) and a discretization step of 0.05 (here, Δ_1 = 0.046875). Thus, the step size of Ju and Farris (1997) is approximately the same as this study, while their computational domain and the total number of elements are both about 4 times as large. Thus, this study could change to M = 64 instead of M = 16, but, as shown in Fig. 2, the diminishing of periodicity effects are negligible for this change of M.

The FFT based methods are compared to the analytical influence coefficients of Eq. (9) and to the low and high Peclet number expressions of Eqs. (10) and (12), respectively. The surface $x_3 = 0$ temperature rise $T = T_1$ from the FRF method is shown in Fig. 4 for the arbitrary Peclet number case because the IFFT, FRF and analytical results are all nearly identical (indistinguishable on a graph like Fig. 4), for each case of Peclet number. In Fig. 4a, the curves for several values of Peclet number $P = P_1$ show that the low Peclet number expressions from Eq. (10) are appropriate for $P < 0.1$ and that the high Peclet number expressions from Eq. (12) are appropriate for $P > 5$. Note that the low Peclet number expression of Eq. (10) and the FFT results must have reference points. The bulk is set for the FFT results by the analytical result from Eq. (9) for $x = -3$, while the bulk is set for the $P = 0$ case by adding 3 to each point's calculated result (to match the $P = 0.01$ value at $x = 0$). In Fig. 4b, the same calculated results are presented, but with a new ordinate. The ordinate $T\sqrt{P}$ is chosen to make the plot more concise; the fast-moving solution of Eq. (12) is graphed once for all Peclet numbers [Johnson (1985); Tichy (1991); Williams (1994)]. Note that Fig. 4b appears to indicate that as the speed increases, the temperature also increases, which is anti-physical and an artifact from the choice of ordinate. Both Fig. 3 and Fig. 4a, which do not have this ordinate, give the correct impression. Finally, it is worth mentioning that some researchers have chosen TP as the ordinate [Jaeger (1942); Carslaw and Jaeger (1959)].

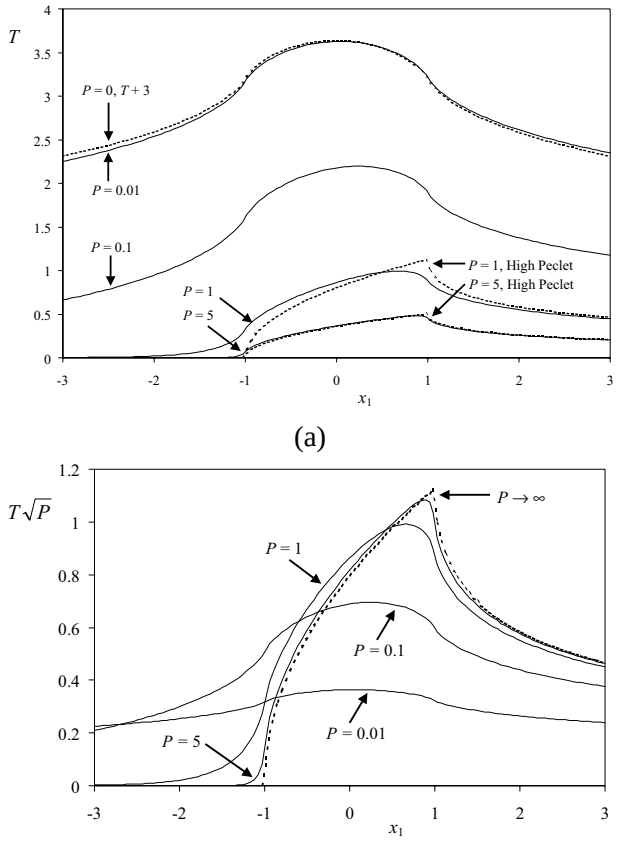

Figure 4 : Homogeneous Line Contact: Length Source. (a) The surface temperature rise is plotted vs. x_1 for various Peclet numbers. The solid lines are the FRF method results, while the dashed lines are the analytical results for low and hight Peclet number. (b) The curves from (a) are multiplied by $\sqrt{P}$, and the fast-moving case is plotted once for all Peclet numbers as $P \to \infty$.

Again, the average absolute errors between pairs of results are given as follows: For all values of P, this error between the FRF method and the analytical solution of Eq. (9) is less than 1.6 (10^{-2}), between the IFFT method and Eq. (9) is less than 2.1 (10^{-2}) and between the FRF

method and the IFFT method is less than 6.0 (10^{-3}). These errors are slightly higher than those for the circular patch case, but the temperature rise is also higher because the width of the heat source is infinite. Also, this heat has only two directions in which to dissipate, which likely leads to an increased need to expand the spatial domain to diminish the periodicity effects. In this light, and since the error of the FRF method is comparable to that of the IFFT method, the FRF method shows promise for use in contact and heat partition problems.

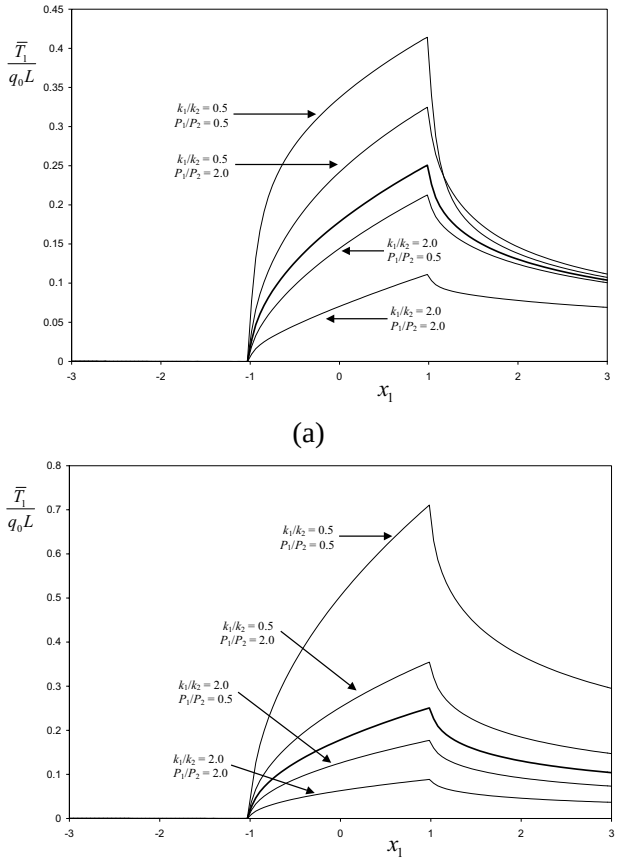

Figure 5 : Coated Line Contact: Fast Moving Case for the Length Source. The FRF method results for the temperature are plotted vs. x_1 in a parameter study with $P_2 = 20$ and $k_2 = 1$. The thicker solid line in the middle is the homogeneous result. (a) $h = 0.1$ (b) $h = 1.0$.

4.3 Parameter Study

The FRF method results for the surface temperature caused by a fast moving line source are shown in Fig. 5 for thickness of (a) $h = 0.1$ and (b) $h = 1.0$. Since the parameter study involves changing k_1 while keeping $k_2 = 1$, the ordinate is $T_1/k_1 = \overline{T}_1/q_0 L$. For comparison with the influence coefficients, which can be found from Eqs. (14) and (12), the substrate Peclet number was chosen to be quite high $P_2 = 20$. Thus even when $P_1/P_2 = 0.5$, $P_1 = 10$, and the fast moving case should still be appropriate. The average absolute errors between the FRF method and the analytical are less than 7.8 (10^{-4}) and 1.5 (10^{-3}) for all cases shown in (a) and (b), respectively. The FRF method results for the surface temperature vs. x_1, with $x_2 = 0$, caused by the line source and the circle source, are shown in Figs. 6 and 7, respectively, with $P_2 = k_2 = 1$. Again the thicknesses are (a) $h = 0.1$ and (b) $h = 1.0$ and the ordinate is $T_1/k_1 = \overline{T}_1/q_0 L$. In Figs. (5) – (7), the thicker solid line shows the homogeneous case

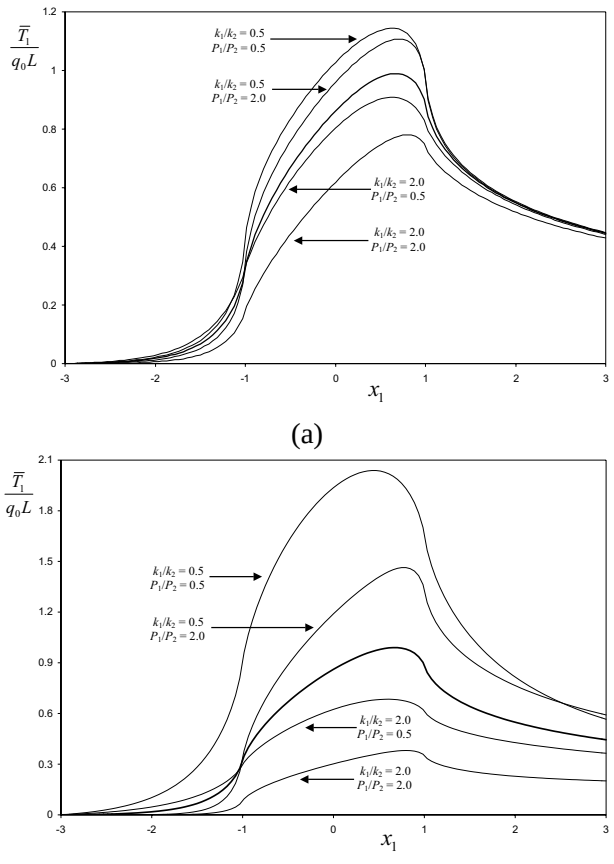

Figure 6 : Coated Line Contact: Length Source. The FRF method results for the temperature are plotted vs. x_1 in a parameter study with $P_2 = k_2 = 1$. The thicker solid line in the middle is the homogeneous result. (a) $h = 0.1$ (b) $h = 1.0$.

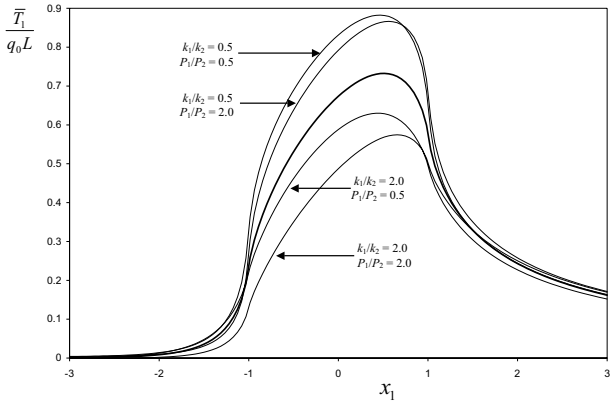

(a)

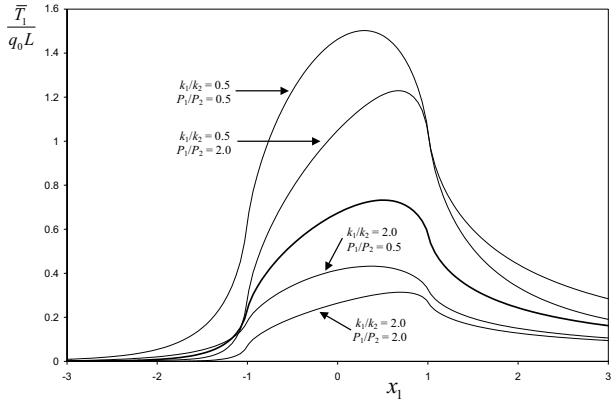

(b)

Figure 7 : Coated Point Contact: Circle Source. The FRF method results for the temperature are plotted vs. x_1 in a parameter study with $P_2 = k_2 = 1$. The thicker solid line in the middle is the homogeneous result. (a) $h = 0.1$ (b) $h = 1.0$.

results. In each of those six figures, two curves are above the homogeneous curve and two curves are below the homogeneous curve. Thus, the parameter study shows that higher surface temperature is associated with lower coating conductivity and lower coating Peclet number. Because the Peclet number is inversely proportional to the diffusivity, higher surface temperature is associated with higher coating diffusivity. Note that the conductivity forces the coated curves to be above or below the homogeneous curve, and therefore the coating conductivity is more important than the coating diffusivity. The effect of the thickness can be seen by comparing parts (a) $h = 0.1$ and (b) $h = 1.0$ of Figs. (5) – (7). The thicker coating cases (b) show temperatures much more spread out from the homogeneous than the thinner coating cases (a) . Thus, the thicker the coating, the more influence it has over surface temperature.

5 Conclusions

Steady-state halfspace and halfplane temperature rise due to frictional heating was studied with fast Fourier transform methods. The Green's functions and influence coefficients found in the literature for special cases were compiled. These cases were used to show the range of applicability of the frequency response functions, which are the Fourier transformed Green's functions and which are found in closed form from Fourier analysis of the governing equations and boundary conditions. The coated halfplane case for the fast-moving heat source was used to perform a brief parameter study of the conductivity and diffusivity ratios. Higher coating conductivity and lower coating diffusivity leads to a decrease in surface temperature. This effect is magnified as the coating thickness increases. In all cases, the results from the FFT based numerical methods and from available analytical expressions showed excellent agreement.

Acknowledgement: The authors wish to thank Shuangbiao Liu, Q. Jane Wang, Sandrine Coulon and Daniel Nelias for their brief consultation in early stages of this work. Also, the comments of the anonymous reviewers are gratefully acknowledged. This work was supported by the National Science Foundation and the Center for Surface Engineering and Tribology.

Nomenclature

$\tilde{g}_j$	Frequency response function.
g_j	Green's function.
G_j	Influence coefficient.
$\overline{h}$	Thickness of the coating, m.
h	Nondimensional thickness of the coating.
$H(x)$	Heaviside unit step function.
i	$\sqrt{-1}$
j	Subscript for coating $(j = 1)$, substrate $(j = 2)$.
k_j	Conductivity, J/m $^\circ$ ks or w/m $^\circ$ k.
L	Half-length of the heat source, m.
M	Frequency refinement factor.
N	Number of nodes in x_1 direction
P_j	Peclet number.
$\overline{q}$	Heat flux, W/m^{2}or N/ms.
q_0	Maximum heat flux, W/m^{2}or N/ms.
q	Nondimensional heat flux.

R	Parameter ratio.
S	Correction sum.
$\overline{T}_j$	Temperature rise, $^\circ$k.
T_j	Nondimensional temperature rise.
U	Speed of the heat flux in the $-x_1$ direction, m/s.
w	Radius in the frequency domain, $w^2=\omega_1^2+\omega_2^2$.
$\overline{x}_m$	Coordinate in $m=1,2,3$ direction, m.
x_m	Nondimensional coordinate in $m=1,2,3$ direction, m.
Δ_1,Δ_2	Nodal spacing in $1,2$ direction.
κ_j	Thermal diffusivity, m^2/s.
η_j	Frequency domain parameter.
ρ	Nondimensional distance.
ω_1,ω_2	Frequency domain counterpart of x_1,x_2

Appendix: Fourier Analysis

The continuous forward and inverse Fourier transform and convolution theorem are:

$$\tilde{F}(\omega)=\int_{-\infty}^{+\infty}F(x)\exp(+\mathrm{i}\omega x)\,dx,$$
$$F(x)=\frac{1}{2\pi}\int_{-\infty}^{+\infty}\tilde{F}(\omega)\exp(-\mathrm{i}\omega x)\,d\omega \tag{A1a}$$

$$\tilde{F}(\omega)=\tilde{g}(\omega)\,\tilde{q}(\omega),$$
$$F(x)=\int_{-\infty}^{+\infty}g(x-y)\,q(y)\,dy \tag{A1b}$$

where ω is the angular frequency and $\tilde{}$ represents a continuous Fourier transformed function [Press, Teukolsky, Vetterling and Flannery (1992)].

The discrete forward and inverse Fourier transform and convolution theorem are [Stein (1997)]:

$$\hat{F}(\omega_n)=\Delta x\sum_{k=0}^{N-1}F(x_k)\exp(+\mathrm{i}\omega_n x_k),$$
$$F(x_k)=\frac{\Delta\omega}{2\pi}\sum_{n=0}^{N-1}\hat{F}(\omega_n)\exp(-\mathrm{i}\omega_n x_k) \tag{A2a}$$

$$\hat{F}(\omega_n)=\hat{G}(\omega_n)\,\hat{q}(\omega_n),$$
$$F(x_k)=\sum_{n=0}^{N-1}G(x_k-x_n)\,q(x_n) \tag{A2b}$$

where $\hat{}$ represents a discrete Fourier transformed function, $\Delta x=L_x/N$, $\Delta\omega=2\pi/L_x$, and

$$x_k=k\Delta x,\quad k=0,\ldots,N-1 \tag{A3a}$$

$$\omega_n=\Delta\omega\cdot\begin{cases}n, & n=0,\ldots,\dfrac{N}{2}\\ (n-N), & n=\dfrac{N}{2}+1,\ldots,N-1\end{cases} \tag{A3b}$$

Following Press, Teukolsky, Vetterling and Flannery (1992) and Liu, Wang and Liu (2000), in Eq. (A2b), the sum in the right equation is a cyclic convolution where $k-n\equiv k-n+N$ if $k<n$, and the transform $\hat{G}(\omega_n)$ in the left equation is the discrete transform of a wrapped-around $G(x_k)$ (i.e. choose x_k as in Eq. (A3b)). In this paper, using Eqs. (A1) – (A2), g is the Green's function and G is the influence coefficient, such that $G(x)=\int_{-\Delta x/2}^{+\Delta x/2}g(x-\xi)\,d\xi$.

Important transform pairs for this paper are given by the following [Campbell and Foster (1931); Rodgers (2001)], with $x_3\geq 0$:

$$\tilde{\tilde{g}}(\omega_1,\omega_2,x_3)=\frac{\exp\left(-x_3\sqrt{\omega_1^2+\omega_2^2+P^2}\right)}{\sqrt{\omega_1^2+\omega_2^2+P^2}},$$
$$g(x_1,x_2,x_3)=\frac{\exp(-P\rho)}{2\pi\rho} \tag{A4a}$$

$$\tilde{g}(\omega_1,x_3)=\frac{\exp\left(-x_3\sqrt{\omega_1^2+P^2}\right)}{\sqrt{\omega_1^2+P^2}},$$
$$g(x_1,x_3)=\frac{1}{\pi}K_0\left(P\sqrt{x_1^2+x_3^2}\right) \tag{A4b}$$

$$\tilde{g}(\omega_1,x_3)=\frac{\exp(-x_3|\omega_1|)}{|\omega_1|},$$
$$g(x_1,x_3)=-\frac{1}{\pi}\ln\sqrt{x_1^2+x_3^2} \tag{A4c}$$

$$\tilde{g}(x_1,\omega_2)=\frac{H(x_1)}{\sqrt{2\pi P x_1}}\exp\left(-\frac{x_1\omega_2^2}{2P}\right),$$
$$g(x_1,x_2)=\frac{H(x_1)}{2\pi x_1}\exp\left(-\frac{Px_2^2}{2x_1}\right) \tag{A4d}$$

$$\tilde{g}(\omega_1,x_3)=\frac{\exp\left(-x_3\sqrt{-2\mathrm{i}P\omega_1}\right)}{\sqrt{-2\mathrm{i}P\omega_1}},$$
$$g(x_1,x_3)=\frac{H(x_1)}{\sqrt{2\pi P x_1}}\exp\left(-\frac{Px_3^2}{2x_1}\right) \tag{A4e}$$

where $\rho=\sqrt{x_1^2+x_2^2+x_3^2}$. Note that an appropriate spa-

tial reference point must be used in Eq. (A4c) to ignore the infinite bulk effect. The transform pairs used in the text follow from applying combinations of Eq. (A4) with the frequency shift formula [Campbell and Foster (1931)]:

$$\tilde{\tilde{h}}(\omega_1) = \tilde{\tilde{g}}(\omega_1 - \mathrm{i}P), \quad h(x_1) = g(x_1)\exp(Px_1) \qquad \text{(A5)}$$

References

Abramowitz, M.; Stegun, I. A. (1972): *Handbook of Mathematical Functions*, Dover Publications, Inc., New York.

Archard, J. F. (1958): The temperature of rubbing surfaces. *Wear*, vol. 2, pp. 438-455.

Blok, H. (1937): Theoretical study of temperature rise at surfaces of actual contact under oiliness conditions. In: *Proc Ins Mech Eng Gen Disc Lubr*, vol. 2, Institution of Mechanical Engineers, London, pp. 222-235.

Blok, H. (1963): The flash temperature concept. *Wear*, vol. 6, pp. 483-493.

Bos, J.; Moes, H. (1995): Frictional heating of tribological contacts. *J Tribol*, vol. 117, pp. 171-177.

Campbell, G. A.; Foster, R. M. (1931): *Fourier Integrals for Practical Applications*, Bell Telephone Laboratories, New York.

Carrier, G. F.; Pearson, C. E. (1988): *Partial Differential Equations: Theory and Technique*, 2nd Edition, Academic Press, San Diego, CA.

Carslaw, H. S.; Jaeger, J. C. (1959): *Conduction of Heat in Solids*, Oxford University Press, London.

Colin, F.; Lubrecht, A. A. (2001): Comparison of FFT-MLMI for elastic deformation calculations. *J Tribol*, vol. 123, pp. 884-887.

Floquet, A. (1985): Les temperatures eclairs en millieu multicouches. *Proc Eurotrib '85 Lyon, France*, vol. 1, paper 4.2.1, pp. 1-6.

Gao, J.; Lee, S.C.; Ai, X.; Nixon, H. (2000): An FFT-based transient flash temperature model for general three-dimensional rough surface contacts. *J. Tribol*, vol. 122, pp. 519-523.

Jaeger, J. C. (1942): Moving sources of heat and the temperature at sliding contacts. *Proc Roy Soc N S W*, vol. 76, pp. 203-224.

Johnson, K. L. (1985): *Contact Mechanics*, Cambridge University Press, Cambridge.

Ju, F. D.; Liu, J. C. (1988): Parameters affecting thermo-mechanical cracking in coated media due to high-speed friction load. *J Tribol*, vol. 110, pp. 222-227.

Ju, Y.; Farris, T. N. (1997): FFT thermoelastic solutions for moving heat sources. *J Tribol*, vol 119, pp. 156-162.

Kennedy, F. E.; Colin, F., Floquet, A.; Glovsky, R. (1984): Improved techniques for finite element analysis of sliding surface temperatures. In: D. Dowson, et al. (eds) *Developments in Numerical and Experimental Methods Applied to Tribology*, Butterworths, London, pp. 138-150.

Leroy, J. M.; Floquet, A.; Villechaise, B. (1989): Thermomechanical behavior of multilayered media: Theory. *J Tribol*, vol. 111, pp. 538-544.

Leroy, J. M.; Floquet, A.; Villechaise, B. (1990): Thermomechanical behavior of multilayered media: Results. *J Tribol*, vol. 111, pp. 317-323.

Ling, F. F. (1973): *Surface Mechanics*, John Wiley and Sons, New York.

Liu, G.; Wang, Q. (1999): A thermoelastic asperity contact model considering steady-state heat transfer. *Tribol Trans*, vol. 42, pp. 763-770.

Liu, G.; Wang, Q.; Liu, S. B. (2001): A three-dimensional thermal-mechanical asperity contact model for two nominally flat surfaces in contact. *J Tribol*, vol. 123, pp. 595-602.

Liu, S. B.; Wang, Q.; Liu, G. (2000): A versatile method of discrete convolution and FFT (DC-FFT) for contact analyses. *Wear*, vol. 243, pp. 101-111.

Polonsky, I. A.; Keer, L. M. (2000): Fast methods for solving rough contact problems: A comparative study. *J Tribol*, vol. 122, pp.36-41.

Polonsky, I. A.; Keer, L. M. (1999): A new numerical method for solving rough contact problems based on the multi-level multi-summation and conjugate gradient technique. *Wear*, vol. 231, pp. 206-219.

Press, W. H.; Teukolsky, S. A.; Vetterling, W. T.; Flannery, B. P. (1992): *Numerical Recipes in Fortran*, 2nd Edition, Cambridge University Press, Cambridge.

Qui, L.; Cheng, H. S. (1998): Temperature rise simulation of three-dimensional rough surfaces in mixed lubrication contact. *J Tribol*, vol. 120, pp. 310-318.

Rodgers, M. J. (2001): Computational methods for solving boundary integral equations in fracture mechanics and contact mechanics. *Ph.D. Dissertation*, Northwest-

ern University, Evanston, IL.

Sneddon, I. N. (1951): *Fourier Transforms*, Dover Publications, Inc., New York.

Stein, S. (1997): *Introduction to Seismology, Earthquakes and Earth Structure*, Northwestern University, Evanston, IL.

Tian, X. (1992): Surface temperature at the contact interface of sliding systems. *Ph.D. Dissertation*, Dartmouth College, Hanover, NH.

Tian, X.; Kennedy, F. E. (1993): Temperature rise at the sliding contact interface for a coated semi-infinite body. *J Tribol*, vol . 115, pp. 1-9.

Tian, X.; Kennedy, F. E. (1994): Maximum and average flash temperatures in sliding contacts. *J Tribol*, vol. 116, pp. 167-174.

Tichy, J. (1991): Closed-form expression for temperature in a semi-infinite solid due to a fast moving surface heat source. *J Tribol*, vol. 113, pp. 828-831.

Vick, B.; Golan, L. P.; Furey, M. J. (1994): Thermal effects due to surface films in sliding contact. *J. Tribol*, vol. 116, pp. 238-246.

Wang, Q.; Cheng, H. S. (1995): A mixed lubrication model for journal bearings with a thin soft coating – Part II: Flash temperature analysis and its application to TiN coated Al-Si bearings. *Tribol Trans*, vol. 38, pp.517-524.

Williams, J. A. (1994): *Engineering Tribology*, Oxford University Press, Oxford.